Patterned cell death sculpts functional and adaptive neural networks in flies

Sinziana Pop[1], Chin-Lin Chen [2], Connor J Sproston[1], Shu Kondo[3], Pavan Ramdya[2]* and Darren W Williams[1]*

[1] Centre for Developmental Neurobiology
King's College London
New Hunt's House 4th Floor
Guy's Hospital Campus
London SE1 1UL
UK

[2] Neuroengineering Laboratory
Brain Mind Institute and Institute of Bioengineering
École Polytechnique Fédérale de Lausanne
CH-1015 Lausanne
Switzerland

[3] Genetic Strains Research Center
National Institute of Genetics
Shizuoka
Japan

*Correspondance should be addressed to:

Telephone: +44 2078486138 (DWW)
+41 21 693 69 60 (PR)

Email: darren.williams@kcl.ac.uk
pavan.ramdya@epfl.ch

1

Summary

Changes to the structure and function of neural networks are thought to underlie the evolutionary adaption of animal behaviours. Among the many development phenomena that generate changes, patterned programmed cell death is thought to play a role. For example, apoptotic cell death is the final fate of 40% of neurons in the developing *Drosophila* central nervous system. Outside the brain, modifications in the patterning of cell death are known to underlie the adaptation of tissue structure and function. However, whether similar modifications also underlie adaptive changes in neural circuitry remains unknown. Here we show that programmed cell death occurs continuously throughout fly neurogenesis, is stereotyped, happens very soon after neurons are born, and is thus a major force sculpting the architecture of neural networks. Blocking cell death permits the emergence of 'undead' neurons which elaborate complex processes into the neuropil and express distinct transmitter phenotypes. Thermogenetic activation of 'undead' neurons drives locomotion, demonstrating that they are functional. *In vivo* recordings of 'undead' neural activity in behaving animals demonstrates their integration into motor networks. Together, these data suggest that the evolutionary modulation of death-based patterning could be used to generate novel network motifs. Consistent with this, a comparative analysis of homologous neuronal populations in flightless dipterans reveals that altered patterns of cell death coincide with the loss of flight.

Nervous systems are exquisitely adapted to the biomechanical and ecological environments in which they operate, and the modifications of neural network architecture is thought to drive adaptive animal behaviours[1]. Such changes can include the modification of transmitter repertoire, excitability, connectivity, or the number of neurons within specific regions of the CNS. Studies comparing the nervous systems of mammalian species that occupy different ecological niches have revealed differences in the number of cells within homologous brain regions[2]. These differences may have occurred through expansions or reductions of cell populations, by changes in neurogenesis, or in apoptotic programmed cell death (PCD) during development[3]. Most studies of nervous system evolution have focused on stem cell identity and differential proliferation dynamics[4–6]. However, in insects, neural progenitor cells that generate central neurons are highly conserved despite a remarkable diversity of body plans[5]. Therefore, other important mechanisms must drive the diversification of insect nervous systems. Here we describe an extensive role for ancient programs of developmental cell death in the patterning of insect central nervous systems (CNS), from primitive firebrats to the most derived true flies.

In insects, the majority of CNS neurons are generated by neural precursor cells called neuroblasts (NBs) [7]. In *Drosophila* and other holometabolous insects, a first wave of neurogenesis generates the larval nervous system[8,9]. Following a period of quiescence the NBs reactivate and produce neurons throughout larval life until the early pupal stages. These newly-born postembryonic neurons extend simple processes into the neuropil and stall until the pupal-adult transition when they grow complex arborisations and synapse with their target cells[10]. Type I NBs bud off a ganglion mother cell (GMC) which undergoes a terminal division to generate 2 neurons with asymmetric cell fates (an A cell and a B cell). When collected together we call these half lineages hemilineage A and hemilineage B (**Fig. 1a, b**). Hemilineages act as functional units in adult flies[11–17]. Previous work has showed that a major fate of postembryonic

neurons is PCD (**Fig. 1b, c**), affecting approximately 40% of hemilineages[16,18] and thus plays a major role in patterning networks.

Until now it has been difficult to study PCD on a cell by cell basis *in vivo,* therefore, to interrogate PCD we developed a new genetically encoded probe called SR4VH that reveals effector caspase activity within cells (**Fig. 1d**). SR4VH consists of a membrane-bound red fluorescent protein (Src::RFP) and a green fluorescent protein with a strong nuclear signal (Venus::H2B) linked together by four tandem repeats of the amino acid sequence DEVD. When effector caspases cleave the DEVD site, Venus accumulates in the nucleus while RFP remains bound to the cell membrane. Using the neuroblast driver *Worniu-GAL4*, we could visualize postembryonic NBs and 10-20 of their most recent progeny (due to GAL4 perdurance). We confirmed that SR4VH is reliable as a reporter for cell death in wandering 3rd instar larvae (wL3) by analysing its expression pattern in all lineages of postembryonic neurons in the thoracic ventral nerve cord (VNC). (**Fig. 1a,** bottom; **Extended Data Fig. 1a**). Previously studies of neuronal PCD have largely focused on its role during metamorphic transitions, where it eliminates differentiated neurons at puparium formation[19] and post eclosion in adults[20,21], both of which are gated by ecdysteroids. In contrast, we found dying cells were associated with lineages in the brain and VNC throughout the whole period of postembryonic neurogenesis (**Fig. 1e, f, g**) which lasts for 3.5 days, from mid 2nd instar (L2) to 12h after pupariation (**Fig. 1h**). As previously suggested[16], the time course of PCD indicates that cells die early – very soon after they are born – and often before they have extended a neuritic process. This death is unlike the 'trophic' PCD found in vertebrates, where a neuron would interact with its target cell and die in the absence of appropriate survival signals. In support of an early onset of PCD, we see sequential stages of cell death, dependent on the distance from the NB (**Fig. 1i, j, k**; **Extended data Fig. 1b**). We conclude that PCD can be

initiated at any point <5 hours after neuron birth and that this rapid and widespread PCD is a crucial part of patterning.

Because PCD selectively eliminates subsets of newly born-neurons in the fruit fly, and the grasshopper[22], we wondered if this same rapid and early PCD takes place during the development of the CNS in the primitive insect the firebrat *Thermobia domestica* (**Fig. 1l, m**). Using TUNEL labelling we found dying cells close to many NBs in all thoracic neuromeres at 50-55% of embryonic development (**Fig. 1n, o, p**). These data suggest that early PCD during neurogenesis may be a universal and ancestral feature that sculpts the nervous system of all insects.

The extent of early PCD during development could be a driver of adaptive neural network variation. To probe its potential for modifying neural networks, we asked if blocking PCD in one doomed hemilineage would permit neurons to survive into adulthood, elaborate neurites, and acquire a neurotransmitter identity. In lineage 0 (produced by the medial NB), hemilineage A survives and is made up of Engrailed-positive cells[17] which differentiate into GABAergic interneurons[12]. Using SR4VH, we found that only Engrailed-negative cells die during postembryonic neurogenesis in wL3 larvae (**Fig. 2a**). Because a small number of hemilineage B cells born in the embryo become octopaminergic, we hypothesised that rescue from PCD would generate more octopaminergic neurons in the postembryonic phase of neurogenesis. Using the *TDC2-GAL4* octopaminergic neuron driver, we observed a 4 to 9-fold increase in the number of octopaminergic neurons in the thoracic VNC of *H99/XR38* adult flies deficient for proapoptotic genes ($hid^{+/-}$, $grim^{+/-}$, $rpr^{-/-}$ and $skl^{+/-}$)[18,19] compared with wild-type control animals (**Fig. 2b, c, d, e**). Alongside *TDC2-GAL4*, 'undead' neurons express the vesicular glutamate transporter, VGlut, (**Fig. 2f, g**) like wild-type neurons[23]. A close inspection of the projection patterns of undead neurons generated using MARCM clones homozygous for the loss-of-function allele $dronc^{\Delta A8}$ (in which PCD is inhibited), revealed that, even though

99 they resemble wild-type neurons in some respects (**Fig. 2h**), undead neurons branch
100 extensively in the neuropil and display variable morphology (**Fig. 2i**; **Extended data Fig. 2**).

101 We next asked if undead neurons are functional. To address this, we tested if activating
102 undead neurons with the temperature-gated ion channel TrpA1 in headless adult animals could
103 elicit behaviours (**Fig. 3a, b, c, d; Supplementary Video 1**). In *TDC2-GAL4* positive control
104 flies, expressing TrpA1 in wild-type embryonic-born octopaminergic neurons, thermogenetic
105 stimulation drove long bouts of locomotion (**Fig. 3e, f; Supplementary Video 1**). Importantly,
106 *UAS-TrpA1* negative control – in the absence of *TDC2-GAL4* – and MARCM control flies –
107 without clones – did not react strongly to temperature elevation (**Fig. 3c, e, f; Supplementary**
108 **Video 1**). We found that the activation of undead neurons expressing TrpA1 caused decapitated
109 males to walk (**Fig. 3d, e, f, g; Supplementary Video 1**). These data are consistent with the
110 observation that octopamine applied to the exposed anterior notum of decapitated flies causes
111 walking[24] and strongly suggests that undead neurons are functional and capable of releasing
112 neurotransmitters in the CNS.

113 To determine if undead neurons are integrated into pre-existing thoracic circuits, we
114 recorded the activity of mixed undead and wild-type octopaminergic neuron populations
115 expressing GCaMP6s – an activity reporter – and tdTomato – an anatomical fiduciary – in
116 intact *H99/XR38* flies during tethered behaviour on a spherical treadmill[25] (**Fig. 4a, b**). We
117 observed conspicuous increases in neural activity during CO_2 stimulation-induced walking in
118 both wild-type controls (**Extended data Fig. 3**) and in *H99/XR38* flies (**Fig. 4c, d, e;**
119 **Supplementary Video 2, 3**). Because undead neurons outnumber their wild-type counterparts
120 by a ratio of 6.5 to 1, we can conclude that both neuronal types are active in *H99/XR38* flies.
121 Confirming this, we observed an increase in GCaMP6s fluorescence across all subregions
122 along the width of the primary neurite bundle (**Extended data Fig. 4; Supplementary Video**
123 **4**).

Our observation that undead neurons functionally integrate into the CNS of adult flies strongly supports the possibility that PCD can be leveraged to modify neural circuits over the course of evolution. Similar programs of PCD are evident within the olfactory sensory system of *Drosophila* where blocking death also results in the integration of new olfactory sensory neurons[26]. To explore this possibility further, we looked for evidence of evolutionary adaptive modifications to PCD. Specifically, we asked whether lineages known to function in flight circuitry might be modified in flightless insects. Using antibodies for Neuroglian, we analysed homologous hemilineages involved in the flight circuits of two flightless dipterans, the swift louse *Crataerina pallida* (**Fig. 5a**) and the bee louse *Braula coeca* (**Fig. 5b**). We found that hemilineages 3B, 5B, 6A, 7B, 11B, 12A and 19B are reduced in bee lice, but not in swift lice (**Fig. 5c, d, e, f**). In swift lice we labelled octopaminergic neurons from hemilineage 0B using antibodies for tyramine β-hydroxylase[27] and found that, unlike flying dipterans, the swift louse has lost segment-specific variability of cell numbers (**Fig. 5g, h, i**). Typically, there are more octopaminergic neurons in the winged mesothoracic segment in flies[28,29], likely because they are required for flight initiation and maintenance[30]. In hemilineage 0A we found a considerably larger number of GABAergic neurons (**Fig. 5j**), suggesting that PCD is responsible for the selective elimination of their octopaminergic siblings following GMC division. To establish this, we then looked for evidence that early PCD takes place during the development of the swift louse CNS. The swift louse is viviparous and we found that, similar to the tsetse fly[10], its neurodevelopment is significantly delayed – its nervous system only acquires dipteran larval features many days after pupariation (**Fig. 5k**). Using EdU to label proliferating cells and immunostaining for active Dcp-1 (**Fig. 5k, l, m**), we found dying cells located close to NBs throughout the 24 days of pupal neurogenesis (data not shown). In lineage 0, which is easily identified by its medial position and projection pattern in the neuropil, we found cell death in thoracic segments at all time points examined, from day 4 after pupariation to day 23 (**Fig. 5l,**

149 **m**). The proximity of dying cells to NBs and the temporal pattern of death suggests that early
150 PCD is responsible for the reduction in the number of octopaminergic cells in lineage 0 in swift
151 lice. Our exploration of homologous lineages in flightless dipterans demonstrates that changes
152 in the extent and pattern of PCD may be adaptive. Extensive reductions in flight hemilineages
153 are consistent with the more derived body plan of bee lice, which have a reduced thorax lacking
154 wings, halteres and scutellum[31]. We found no change in the morphology of thoracic lineages
155 in swift lice, yet early PCD is widespread during development and likely targets hemilineage
156 B neurons in lineage 0. Because swift lice are unable to fly but have vestigial wings and
157 halteres[32,33], such hemilineage-specific subtle changes in cell numbers are suggestive of an
158 intermediate level of reduction.

159 In *Drosophila*, we found that undead neurons function. It is possible that by blocking
160 PCD we have reawakened ancestral octopaminergic neurons in lineage 0 – homologous across
161 all insects[34,35]. Other hemilineages such as 7A may have never existed as mature neurons in
162 the ancestral insect CNS and may have always had a PCD fate. In such cases, it would be
163 interesting to explore what the fate of undead neurons might be and whether they might act as
164 a substrate for evolutionary processes[36]. We have shown that early PCD is adaptive and
165 widespread during neurodevelopment in the CNS of insects, from the primitive firebrats, to
166 true flies. A future challenge will be to elucidate how a given pattern of cell death can be
167 established in such populations and how they can be modified over the course of evolution.
168

169 **Acknowledgements**

170 We would like to thank Richard Benton and Lucia Prieto-Godino for discussions and sharing
171 data. We thank Kristin White and Bloomington Drosophila Stock Center (NIH P40OD018537)
172 for sharing flies; Maria Monastirioti, Hermann Aberle, Ilan Davis and Developmental Studies
173 Hybridoma Bank (NICHD of the NIH, University of Iowa) for antibodies. We are indebted to

Simon Evans, Richard Newell and Bill Murrells for their kind help in collecting swift lice and Andrew Abrams for sending us bee lice. We would like to thank Ian Wynne for his camera. We also thank Matthias Landgraf, David Shepherd and Jon Clarke for reading the manuscript.

Author contributions

D.W. and S.P. conceived the study. D.W., and S.P., designed the experiments apart from *in vivo* imaging. S.P., performed the experiments apart from *in vivo* imaging. P.R. and C.C. conceived and performed the *in vivo* imaging experiment. S.K. designed and made the genetically encoded caspase reporter SR4VH. C.S. generated the *T.domestica* data. S.P. and D.W. collected *C.pallida* in the field. D.W., and S.P.., wrote the first draft of the manuscript and P.R. and S.K. edited the final drafts.

Methods

Animals

We used the following *Drosophila melanogaster* stocks: *Worniu-GAL4; Dr/TM3, Ubx-LacZ, Sb* (BL 56553), *Tdc2-GAL4* (BL 9313), *OK371-GAL4* (BL 26160), *UAS-SR4VH* (described here), *UAS-CD8::GFP* (BL 5137), *UAS-tdTomato-p2A-GCaMP6s*[25] (kind gift from M. Dickinson), *H99/TM3, Sb* (BL 1576), *XR38/TM3*, Sb[37], *If/CyO; dronc*$^{\Delta A8}$*, FRT2A/TM6β, Tb, Hu*[38] and *hs-flp; ; TubP-GAL80, FRT2A/TM3, Sb*[16].

Firebrat adults of *Thermobia domestica* were obtained from Buzzard Reptile and Aquatics (buzzardreptile.co.uk) and reared on a diet of fish flakes and wholemeal bran at 40°C in darkness inside a humid plastic container. A staging series was calculated by time to hatching.

Crataerina pallida swift louse fly adults were collected from swift (*Apus apus*) nesting boxes fitted behind the louvres of belfry windows from churches in Cambridgeshire and Suffolk, UK.

198 Swift lice were kept at 20°C on a 12h dark:12h light cycle until dissected. Pregnant females,
199 recognised by their enlarged and translucent abdomen through which larvae or prepupae could
200 be detected (Fig. 5a), were kept separately and checked daily for pupa ejection. The day in
201 which a pupa was laid was defined as 'Day 0' of external development (outside the mother's
202 abdomen).

203 *Braula coeca* bee louse adults were obtained from a black bee (*Apis mellifera mellifera*) colony
204 on the Isle of Colonsay, UK (kind gift from A. Abrahams). Bee lice were shipped by post in
205 small cages containing worker bees feeding on bee fondant. The black bees and bee lice were
206 anesthetised by placing the cage on a CO_2 pad and the bee lice were removed for dissection.

207

208 **Construction of *UAS-SR4VH***

209 SR4VH was constructed by standard molecular biology procedures. It comprises the
210 myristylation signal of *Drosophila* Src64B (amino acids 1-95), a monomeric red fluorescent
211 protein mRFP1[39], a linker that contains four DEVD sites, a yellow florescent protein Venus[40],
212 and a nuclear localization signal of *Drosophila* histone H2B (amino acids 1-51). While the
213 design is similar to the previously reported caspase probe Apoliner[41], the Src64B myristylation
214 signal and the H2B NLS offers better membrane and nuclear localization, respectively, and
215 four DEVD sites are expected to provide higher sensitivity. The probe was cloned in
216 pUAST[42]and introduced into the *Drosophila* genome by P element-mediated transformation.

217

218 **Immunohistochemistry and chemical staining**

219 *Drosophila* larvae were dissected in PBS without anaesthesia. Firebrat embryos were removed
220 from their chorion and dissected using minuten pins. *Drosophila*, swift louse and bee louse

adults were anesthetised on ice, briefly submerged in absolute ethanol and dissected in PBS. Swift louse pupae were immobilised on double sided sticky tape, removed from their pupal case using forceps and dissected in PBS without anaesthesia. Samples were fixed in 3.6% paraformaldehyde in PBS for 30 min (larvae and pupae) or 1h (adults), washed 3 times in 0.3% PBST (0.3% Triton-X100 in PBS, Sigma-Aldrich), blocked in 5% goat serum (Sigma-Aldrich) in PBST for 1h and incubated with primary antibodies in block for 1-3 days at 4°C (*Drosophila*, bee lice, swift louse pupae), room temperature (firebrats) or 37°C to increase antibody penetration (swift louse adults; block supplemented with 0.02% NaN_3 to prevent microbial growth). Samples were then washed 4 times throughout the day in PBST and incubated with secondary antibodies in block for a further 1-3 days, followed by final washes in PBST and PBS. Brains and VNCs were mounted on poly-L-lysine-coated coverslip, dehydrated in increasing serial concentrations of ethanol (15%, 30%, 70%, 80%, 90% and twice in 100%) for 5min each, dipped once in xylene, then incubated twice for 5min in fresh xylene. A droplet of DePeX (EMS) was added on top of the mounted sample and the coverslip was placed face-down on a glass slide.

We used the following primary antibodies: chicken anti-GFP (1:500; ab13970, Abcam), mouse anti-Neuroglian (1:50; BP 104, Developmental Studies Hybridoma Bank), rabbit anti-cleaved *Drosophila* Dcp1 (1:100; Asp216, Cell Signaling), guinea pig anti-Syncrip (1:100; kind gift from I. Davis; to label neuroblasts and early progeny in lineages - Jim Truman, personal communication), mouse anti-Engrailed/Invected (1:2; 4D9, Developmental Studies Hybridoma Bank), rabbit anti-DVGLUT C-terminus[43] (1:5000; AB_2490071, kind gift from H. Aberle), rat anti-tyramine β-hydroxylase[27] (1:50; TBH, kind gift from M. Monastirioti) and rabbit anti-GABA (1:100; AB_572234, Imunostar).

Secondary antibodies were Alexa Fluor® 488-conjugated goat anti-chicken (1:500; A11039, Invitrogen, Thermo Fisher Scientific), Alexa Fluor® 488-conjugated goat anti-rabbit (1:500;

A11070, Invitrogen, Thermo Fisher Scientific), Cy™3-conjugated donkey anti-rabbit (1:500; 711-006-152, Jackson ImmunoResearch), Cy™5-conjugated donkey anti-mouse (1:500; 715-006-151, Jackson ImmunoResearch), Alexa Fluor® 488-conjugated donkey anti-rat cross-adsorbed against mouse (1:100; 712-545-153, Jackson ImmunoResearch), Alexa Fluor® 488-conjugated donkey anti-guinea pig (1:500; A11073, Invitrogen, Thermo Fisher Scientific).

In firebrat embryos we detected dying cells using the Click-iT Plus TUNEL assay kit (C10618, *life* technologies). To stain cell nuclei and neuropil, firebrat samples were incubated with DAPI (1:10000; D9542, Sigma-Aldrich) and Phalloidin-488 (1:100, *life* technologies) in PBST for 30 min at room temperature. Incubations were carried out following secondary antibody treatment. Samples were then washed in PBST and PBS, and mounted.

EdU treatment

To label proliferating cells and their progeny we used the Click-iT EdU imaging Kit (C10337, *life* technologies). Freshly dissected nervous systems from swift louse pupae were incubated in EdU 1:1000 in PBS at room temperature for 1-3h on a shaker, rinsed with PBS and fixed in cold buffered formaldehyde 3.6% in PBS for 30min. Samples were then stained using the immunohistochemistry protocol described above. The colour reaction for EdU was carried out as instructed by the vendor after the secondary antibodies were washed out.

Generation of Undead neuron MARCM clones

To induce mitotic clones of undead neurons, rescued from programmed cell death, we used the mosaic analysis with a repressible cell marker technique[44]. 0-4h first instar larvae resulting from crossing females of the genotype *hs-flp; ; TubP-GAL80, FRT2A/TM3, Sb* with *; TDC2-*

GAL4, UAS-CD8::GFP, UAS-TrpA1; dronc$^{\Delta A8}$, FRT2A/TM6β, Tb, Hu males were heat-shocked at 37°C in a plastic food vial placed in a water bath for either 1h or 45min, followed by 45min at room temperature and a second incubation period at 37°C for 30min. After heat-shock, larvae were immediately returned to 23 or 25°C. Cell death was blocked in clones homozygous for the loss-of-function allele of the initiator caspase dronc. Because we used the octopaminergic driver line *TDC2-GAL4* to induce the expression of CD8::GFP and TrpA1, we were able to visualise and thermogenetically activate only postembryonic neurons of hemilineage 0B. A small number of wild-type octopaminergic neurons are born during postembryonic neurogenesis (1 in T1 and T3, 4-5 in T2, data now shown). To ensure the characterisation of undead neurons only, MARCM clones including a bilaterally symmetrical primary neurite were excluded from analysis.

Thermogenetic activation and video recordings

Prior to recordings, 2-6-day-old males of *Drosophila melanogaster* (*hs-flp/+; Tdc2-GAL4, UAS-CD8::GFP, UAS-dTRPA1/+; dronc$^{\Delta A8}$, FRT2A/TubP-GAL80, FRT2A*) reared at 23 or 25°C in a 12h:12h light:dark cycle were anesthetised on ice and decapitated using a pair of micro spring scissors in under 3min. We used males as we found they are more responsive to octopamine release by thermogenetic activation than females (data not shown). The headless flies were brushed back into a food vial placed on its side and left to recover for at least 1 hour. To generate the heat ramp required to thermogenetically activate undead neurons, we used a 12V thermoelectric Peltier plate (model: TEC1-12706, size: 40mm x 40mm x 3.6mm) connected to a DC power supply (HY3005D, Rapid Electronics) set at a constant current of 0.46A, with a variable voltage, calibrated using an infrared laser thermometer (N92FX, Maplin). These settings generated a temperature ramp which lasted 70s from 22°C to 34°C.

Videos were recorded at 25fps using a Sony NEX-5N digital camera (kindly provided by Ian Wynne) mounted to a stereo microscope. A piece of graph paper was used for spatial calibration. To match the presence of undead neurons with behaviour, each decapitated fly used for thermogenetic activation was indexed and prepared for dissection and immunostaining.

Two-photon calcium imaging in behaving intact flies

The method for *in vivo* two-photon imaging of the VNC in behaving adult *Drosophila* is described in[25]. Briefly, flies were anesthetised through cooling and then mounted onto custom imaging stages. The dorsal thoracic cuticle was removed and indirect flight muscles were left to degrade over the course of 1h. Subsequently, the proventriculus and salivary glands were resected to gain optical access to the VNC.

Horizontal sections of the T1 leg ganglion were imaged using galvo-galvo scanning. For control animals, the bifurcation point of TDC-positive neurites were imaged to circumvent ROI disappearances caused by movement. For animals harbouring undead *TDC2-GAL4*-positive neurons, the thickest branch of the axonal bifurcation was chosen because they were most likely to contain undead neurites. Image dimensions ranged between 512×512 and 320×320, resulting in 1.6 to 3.4 fps data acquisition. Imaging areas ranged between 92×92 µm and 149×149 µm. Laser power was held at ~8 mW.

Data analysis for 2-photon imaging in behaving *Drosophila*

Python scripts (modified from[25]) were used to extract ROI fluorescence traces and to compute spherical treadmill ball rotations. Walking epochs were determined by placing a threshold on ball rotations, which were first converted into anterior-posterior ($v_{forward}$) and medial-lateral

(v_{side}) speeds (1 rot s^{-1} = 31.42 mm s^{-1}) and into degrees s^{-1} (1 rot s^{-1} = 360° s^{-1}) for yaw ($v_{rotation}$) movements. Thresholds were 0.12 mm, 0.12 mm, and 5 degrees, respectively. Periods below these thresholds were considered 'resting' while other periods were considered 'walking'. Fluorescence traces for epochs with the same behavior were aligned by start point to compute average %ΔR/R traces for specific actions.

To calculate fluorescence traces for small subregions-of-interest across neuritic bundles containing both undead and wild-type neurites, images were registered using an optic flow method described in[25]. This registration served to minimize motion artefacts. Analysis was limited to a period with no warping artefacts and no ROI disappearance. Subregions were manually selected as small circular ROIs across the neuritic bundle of the registered image. Fluorescence values were then computed from each sub-ROI.

Confocal imaging and image processing

Images were acquired using a Zeiss LSM 510 or a Zeiss LSM 800 confocal microscope at a magnification of 20x or 40x with optical sections taken at 1µm intervals. The resulting images were examined and processed using Fiji (https://imagej.net/Fiji). Some images were manually cropped using the Freehand Selection tool to remove debris or to cut out neuronal lineages in *; Worniu-GAL4, UAS-SR4VH;* samples (Fig. 1c).

Fluorescence intensity plots

To generate fluorescence intensity along Line plots, we used the Plot Profile tool in Fiji to extract raw fluorescence intensity values for the RFP and Venus channels. The values were imported into MATLAB (R2018a, MathWorks) and normalised by dividing all fluorescence

intensity values to the maximum value encountered along each Line. In this manner, all fluorescence intensity along Line plots have a common scale from 0 to 1, with 1 being the highest value encountered along that Line.

Analysis of thermogenetic activation

Decapitated flies were considered to be walking if they covered a distance greater than 1 body length and moved their legs in a coordinated sequence from T3 to T2 to T1 at least once on each siderefHarris2012. Forward, backward and sideway movements were all interpreted as walking when both aforementioned conditions were respected. To generate fly body traces video recordings were imported in MATLAB (R2018a, MathWorks) and the centroid of the decapitated fly (located on the scutellum) was extracted from each frame using a custom-written script. Each frame was converted into a grayscale image, its contrast enhanced using contrast-limited adaptive histogram equalization, filtered using a gaussian smoothing kernel with a standard deviation of 4, binarized using a custom threshold and the geometric centre of the fly body automatically extracted and stored in an array. To confirm that the centroid detection was accurate, a red dot with the centroid coordinates was superimposed onto each frame of the original recording and the annotated movie was saved for manual inspection.

Quantification of 3A/3B bundle diameters

For calculating 3A/3B hemilineage bundle diameter ratios in fruit flies and bee lice, we generated transverse rendered maximum intensity projections of inverted grayscale confocal stacks for the pro- and mesothorax (T1 and T2) and frontal projections for the metathorax (T3). Optical sections were selected to include the common lineage bundle and the individual hemilineage bundles after their split. Diameter measurements were taken at the widest point

within 5 µm of the bundle split using the Straight Line tool in Fiji and ratios were calculated by dividing the diameter of hemilineage 3A to that of 3B.

Statistical analysis

For comparing neuron numbers, 3A/3B bundle diameter and T2/T1 number of neurons, data was tested for normal distribution using the Kolmogorov-Smirnov test and visualisation of Normal Q-Q plots. Differences between groups were analysed using either the independent samples t-test for normally distributed data, Welch's test if data failed to meet the homogeneity of variances assumption or Mann-Whitney t-tests if data failed to meet the normality and homogeneity of variances assumptions of the independent samples t-test.

For comparing the number of flies which walked in each experimental group, we performed a Pearson chi-squared test and interpreted the resulting exact significance if the minimum expected count was greater than 5, or the Fisher's Exact Test 2-sided significance if the minimum expected count was lower than 5 in at least one cell of the contingency table. To correct for multiple comparisons we performed a Bonferroni correction (i.e. p values were multiplied by 6, the total number of pairwise tests).

All statistical tests were performed in SPSS Statistics 23 (IBM) with an α set at 0.05. In all figures, bars represent means ± standard deviation; $P^{*} < 0.05$, $P^{***} < 0.001$, P^{ns} = not significant.

Data availability

All data generated in this study are available upon request from the corresponding authors.

386 **References**

387 1. Katz, P. S. Evolution and development of neural circuits in invertebrates. *Curr Opin*
388 *Neurobiol* **17,** 59–64 (2007).

389 2. Herculano-Houzel, S., Manger, P. R. & Kaas, J. H. Brain scaling in mammalian evolution
390 as a consequence of concerted and mosaic changes in numbers of neurons and average
391 neuronal cell size. *Front Neuroanat* **8,** 77 (2014).

392 3. Charvet, C. J., Striedter, G. F. & Finlay, B. L. Evo-devo and brain scaling: candidate
393 developmental mechanisms for variation and constancy in vertebrate brain evolution.
394 *Brain Behav Evol* **78,** 248–257 (2011).

395 4. Rakic, P. Evolution of the neocortex: a perspective from developmental biology. *Nat Rev*
396 *Neurosci* **10,** 724–735 (2009).

397 5. Truman, J. W. & Ball, E. E. Patterns of embryonic neurogenesis in a primitive wingless
398 insect, the silverfish, Ctenolepisma longicaudata: comparison with those seen in flying
399 insects. *Dev Genes Evol* **208,** 357–368 (1998).

400 6. Biffar, L. & Stollewerk, A. Conservation and evolutionary modifications of neuroblast
401 expression patterns in insects. *Dev Biol* **388,** 103–116 (2014).

402 7. Bate, M. C. Embryogenesis of an insect nervous system I. A map of the thoracic and
403 abdominal neuroblasts in Locusta migratoria. *Journal of Embryology and Experimental*
404 *Morphology* **35,** 107–123 (1976).

405 8. Booker, R. & Truman, J. W. Postembryonic neurogenesis in the CNS of the tobacco
406 hornworm, Manduca sexta. I. Neuroblast arrays and the fate of their progeny during
407 metamorphosis. *J Comp Neurol* **255,** 548–559 (1987).

408 9. Truman, J. W. & Bate, M. Spatial and temporal patterns of neurogenesis in the central
409 nervous system of Drosophila melanogaster. *Dev Biol* **125,** 145–157 (1988).

410 10. Truman, J. W. Metamorphosis of the central nervous system of Drosophila. *J Neurobiol*
411 **21,** 1072–1084 (1990).

412 11. Harris, R. M., Pfeiffer, B. D., Rubin, G. M. & Truman, J. W. Neuron hemilineages provide
413 the functional ground plan for the Drosophila ventral nervous system. *elife* **4,** (2015).

12. Lacin, H. *et al.* Neurotransmitter identity is acquired in a lineage-restricted manner in the Drosophila CNS. *elife* **8,** (2019).

13. Lin, S. *et al.* Lineage-specific effects of Notch/Numb signaling in post-embryonic development of the Drosophila brain. *Development* **137,** 43–51 (2010).

14. Shepherd, D., Sahota, V., Court, R., Williams, D. W. & Truman, J. W. Developmental organisation of central neurons in the adult drosophila ventral nervous system. *J Comp Neurol* (2019).

15. Shepherd, D., Harris, R., Williams, D. & Truman, J. W. Postembryonic Lineages of the Drosophila Ventral Nervous System: Neuroglian expression reveals the adult hemilineage associated fiber tracts in the adult thoracic neuromeres. *J Comp Neurol* **524,** 2677–2695 (2016).

16. Truman, J. W., Moats, W., Altman, J., Marin, E. C. & Williams, D. W. Role of Notch signaling in establishing the hemilineages of secondary neurons in Drosophila melanogaster. *Development* **137,** 53–61 (2010).

17. Truman, J. W., Schuppe, H., Shepherd, D. & Williams, D. W. Developmental architecture of adult-specific lineages in the ventral CNS of Drosophila. *Development* **131,** 5167–5184 (2004).

18. Kumar, A., Bello, B. & Reichert, H. Lineage-specific cell death in postembryonic brain development of Drosophila. *Development* **136,** 3433–3442 (2009).

19. Truman, J. W., Talbot, W. S., Fahrbach, S. E. & Hogness, D. S. Ecdysone receptor expression in the CNS correlates with stage-specific responses to ecdysteroids during Drosophila and Manduca development. *Development* **120,** 219–234 (1994).

20. Draizen, T. A., Ewer, J. & Robinow, S. Genetic and hormonal regulation of the death of peptidergic neurons in the Drosophila central nervous system. *Dev Neurobiol* (1999).

21. Kimura, K. I. & Truman, J. W. Postmetamorphic cell death in the nervous and muscular systems of Drosophila melanogaster. *J Neurosci* **10,** 403–401 (1990).

22. Jia, X. X. & Siegler, M. V. Midline lineages in grasshopper produce neuronal siblings with asymmetric expression of Engrailed. *Development* **129,** 5181–5193 (2002).

23. Greer, C. L. *et al.* A splice variant of the Drosophila vesicular monoamine transporter contains a conserved trafficking domain and functions in the storage of dopamine, serotonin, and octopamine. *J Neurobiol* **64,** 239–258 (2005).

24. Yellman, C., Tao, H., He, B. & Hirsh, J. Conserved and sexually dimorphic behavioral responses to biogenic amines in decapitated Drosophila. *Proc Natl Acad Sci U S A* **94,** 4131–4136 (1997).

25. Chen, C. L. *et al.* Imaging neural activity in the ventral nerve cord of behaving adult Drosophila. *BioRxiv* (2018).

26. Prieto-Godino *et al*. Functional integration of "undead" neurons in the olfactory system. (2019).

27. Monastirioti, M., Linn, C. E. & White, K. Characterization of Drosophila tyramine beta-hydroxylase gene and isolation of mutant flies lacking octopamine. *J Neurosci* **16,** 3900–3911 (1996).

28. Monastirioti, M. *et al.* Octopamine immunoreactivity in the fruit fly Drosophila melanogaster. *J Comp Neurol* **356,** 275–287 (1995).

29. Schlurmann, M. & Hausen, K. Mesothoracic ventral unpaired median (mesVUM) neurons in the blowfly Calliphora erythrocephala. *J Comp Neurol* **467,** 435–453 (2003).

30. Roeder, T. Tyramine and octopamine: ruling behavior and metabolism. *Annu Rev Entomol* **50,** 447–477 (2005).

31. Imms, A. D. On Braula coeca Nitsch and its affinities. *Parasitology* **34,** 88 (1942).

32. Bequaert, J. C. The Hippoboscidae or Louse-Flies (Díptera) of Mammals and Birds. Part I. Structure, Physiology and Natural History. *Entomologica Americana* **32,** 1–209 (1952).

33. Hagan, H. R. in *Embryology of the Viviparous Insects* 159–205 (The Ronald Press Company, 1951).

34. Stevenson, P. A. & Spörhase-Eichmann, U. Localization of octopaminergic neurones in insects. *Comp Biochem Physiol A Physiol* **110,** 203–215 (1995).

35. Witten, J. L. & Truman, J. W. Distribution of GABA-like immunoreactive neurons in insects suggests lineage homology. *J Comp Neurol* **398,** 515–528 (1998).

36. Konstantinides, N., Degabriel, S. & Desplan, C. Neuro-evo-devo in the single cell sequencing era. *Current Opinion in Systems Biology* **11,** 32–40 (2018).

37. Peterson, C., Carney, G. E., Taylor, B. J. & White, K. reaper is required for neuroblast apoptosis during Drosophila development. *Development* **129,** 1467–1476 (2002).

38. Kondo, S., Senoo-Matsuda, N., Hiromi, Y. & Miura, M. DRONC coordinates cell death and compensatory proliferation. *Mol Cell Biol* **26,** 7258–7268 (2006).

39. Campbell, R. E. *et al.* A monomeric red fluorescent protein. *Proc Natl Acad Sci U S A* **99,** 7877–7882 (2002).

40. Nagai, T. *et al.* A variant of yellow fluorescent protein with fast and efficient maturation for cell-biological applications. *Nat Biotechnol* **20,** 87–90 (2002).

41. Bardet, P. L. *et al.* A fluorescent reporter of caspase activity for live imaging. *Proc Natl Acad Sci U S A* **105,** 13901–13905 (2008).

42. Brand, A. H. & Perrimon, N. Targeted gene expression as a means of altering cell fates and generating dominant phenotypes. *Development* **118,** 401–415 (1993).

43. Mahr, A. & Aberle, H. The expression pattern of the Drosophila vesicular glutamate transporter: a marker protein for motoneurons and glutamatergic centers in the brain. *Gene Expr Patterns* **6,** 299–309 (2006).

44. Lee, T. & Luo, L. Mosaic analysis with a repressible cell marker for studies of gene function in neuronal morphogenesis. *Neuron* **22,** 451–461 (1999).

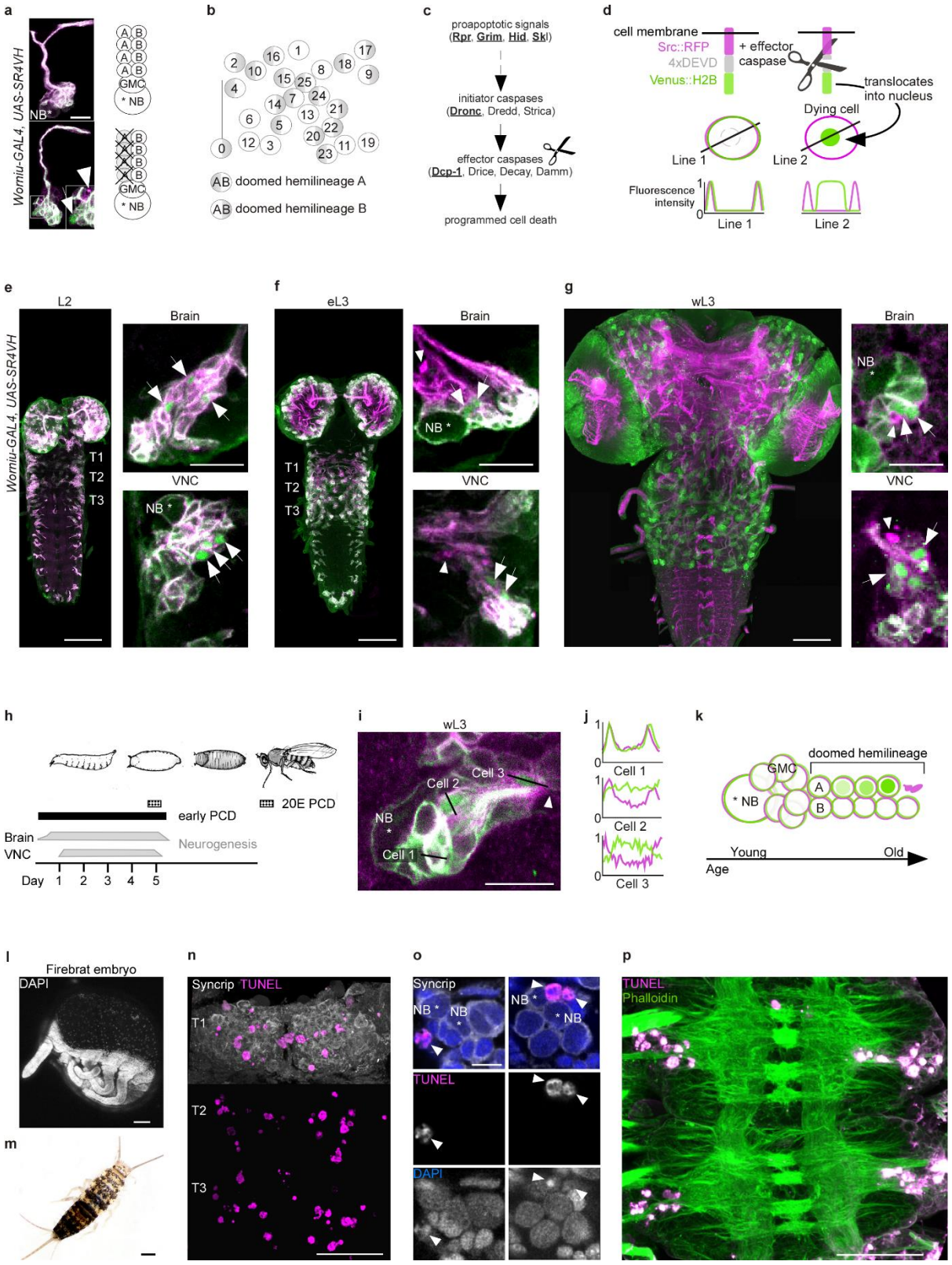

Figure 1 | Early programmed cell death eliminates newly-born neurons in *Drosophila* and the primitive wingless firebrat.

a, Digitally cropped maximum intensity projections of lineage 12 expressing *UAS-SR4VH* driven by *Worniu-GAL4* in the mesothorax (top) and metathorax (bottom) alongside schematics representing lineages consisting of a neuroblast (NB), ganglion mother cells (GMCs), hemilineage A and hemilineage B. Hemilineage 12A undergoes PCD in T3 (bottom). Arrow indicates dying cell, arrowhead indicates RFP-positive dead cell membranes. Scale bar, 10 µm.

b, Schematic representation of the pattern of hemilineage-specific cell death in one hemisegment in the mesothorax.

c, Schematic of PCD in *Drosophila*. Elements disrupted in this study, or used as a PCD readout are underlined.

d, Schematic of effector caspase reporter SR4VH (top) and idealised fluorescence patterns in two cells with distinct caspase activity (bottom): RFP (magenta) and Venus (green) present in the cell membrane (Line 1) versus RFP at the cell membrane and Venus accumulation in the nucleus of a cell undergoing programmed cell death (PCD) (Line 2).

e, **f**, **g**, SR4VH driven by *Worniu-GAL4* reveals dying cells in the central nervous system (CNS) throughout postembryonic neurogenesis in a 2nd instar (**e**, n = 9), early 3rd instar (**f**, n = 8) and wandering 3rd instar (**g**, n = 18) larva. Right panels show examples of lineages with dying cells located close to the NB (*) in the brain (top) and ventral nerve cord (VNC, bottom). Arrows indicate dying cell, arrowheads indicate RFP-positive dead cell membranes. Scale bars, 50 µm (left panels), 10 µm (right panels).

h, Schematic representing the periods of neurogenesis (grey), early PCD (black) and 20-Hydroxyecdysone-dependent PCD (20E PCD, stippled) in *Drosophila* during postembryonic development.

i, SR4VH driven by *Worniu-GAL4* reveals younger cells at earlier stages of cell death (Cell 2) are located closer to the NB than older cells at later stages of cell death (Cell 3), which are closer to the lineage bundle (arrowhead). Image represents a single optical section. Scale bar, 10 µm.

j, Fluorescence intensity profiles (normalised to the maximum value along the line for each channel) plotted along the lines indicated in **i**.

k, Schematic representing successive stages of cell death correlated with distance from NB and cell age in doomed lineages as reported with SR4VH.

l, Maximum intensity projection of DAPI staining in a wholemount firebrat embryo (*Thermobia domestica*) at 50-55% of embryonic development. Scale bar, 100 µm.

m, Adult firebrat. Scale bar, 1mm.

n, Dying cells in the thoracic VNC of a firebrat embryo labelled using TUNEL (magenta) and Syncrip antibodies. Scale bar, 50 µm.

o, Dying cells (arrowheads) are located close to NBs (*). Scale bar, 10 µm.

p, Dying cells (magenta, TUNEL) are located in the cortex of the VNC, where neurogenesis takes place, and not in the neuropil (green, Phalloidin) in a firebrat embryo. Scale bar, 50 µm.

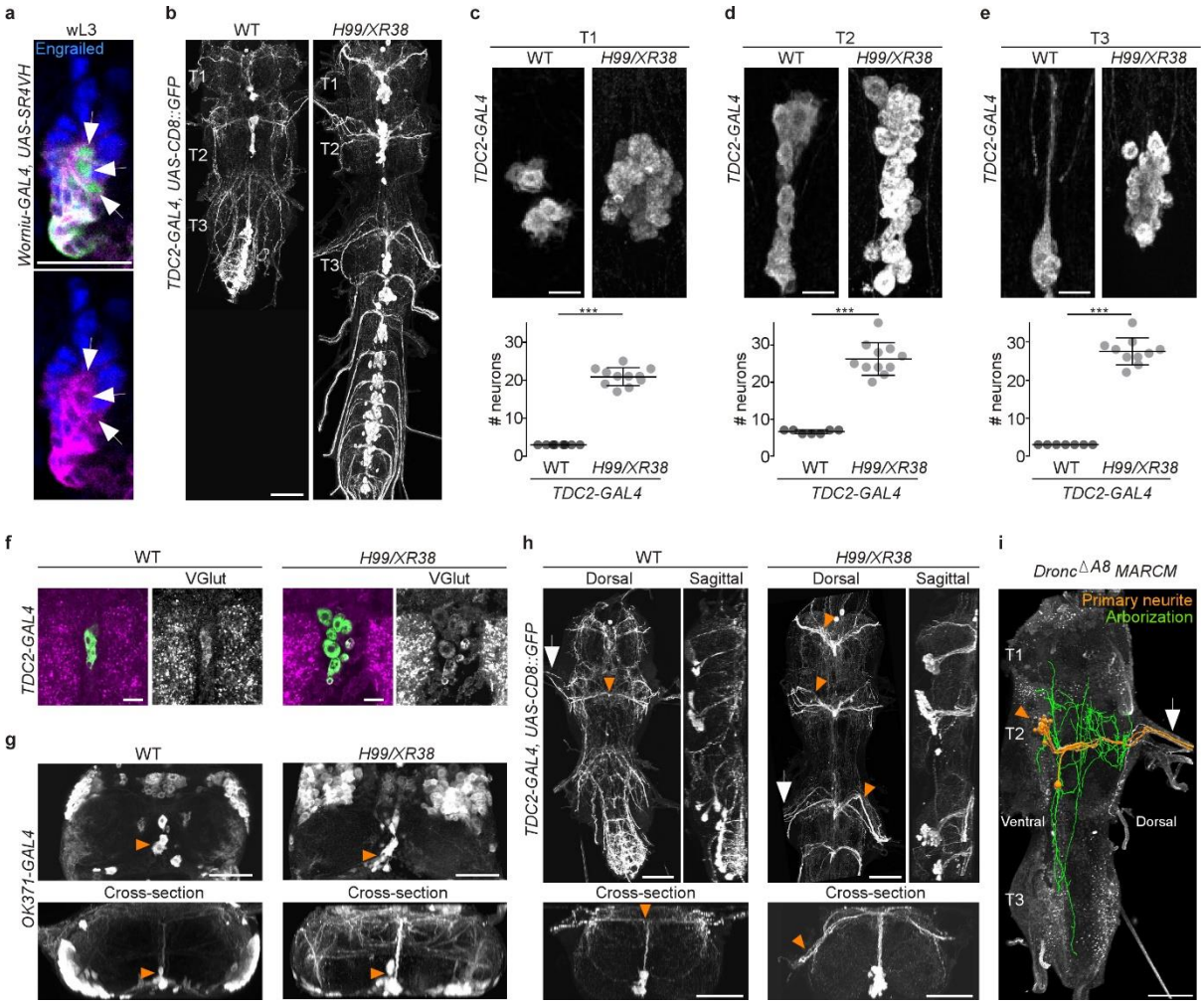

Figure 2 | Undead neurons in hemilineage 0B become octopaminergic, elaborate neurites and join thoracic nerves.

a, SR4VH driven by *Worniu-GAL4* together with antibodies for Engrailed (blue) reveal that only Engrailed-negative cells from hemilineage 0B undergo PCD (white arrowheads) during postembryonic development in the thoracic VNC. Scale bar, 10 µm. *n* = 6.

b, CD8::GFP expression driven by *TDC2-GAL4* in octopaminergic neurons from hemilineage 0B in the VNC of wild-type (WT, left) and PCD-blocked adult flies (*H99/XR38* deficient for $hid^{+/-}$, $grim^{+/-}$, $rpr^{-/-}$ and $skl^{+/-}$, right). *H99/XR38* flies have an enlarged abdominal ganglion resulting from blockage of PCD in NBs, a process which differs from early PCD of newly-born neurons. Scale bar, 50 µm.

c, **d**, **e**, Quantifications of the number of *TDC2-GAL4*-positive octopaminergic neurons in the VNC of WT and *H99/XR38* adult flies. Bars represent mean ± standard deviation. ***P = 0.0002 in T1, ***P = 0.0004 in T2, ***P = 0.0004 in T3, Mann-Whitney. Scale bar, 10 µm. *n* = 11 each.

f, **g**, Antibodies for the vesicular glutamate transporter VGlut and GFP expression driven by the glutamatergic driver line *OK371-GAL4* label both WT and undead (*H99/XR38*) octopaminergic neurons. Orange arrowheads indicate cell bodies. Scale bars, 10 µm (**f**), 50 µm (**g**).

h, CD8::GFP expression driven by *TDC2-GAL4* in WT and *H99/XR38*. WT and undead primary neurites project dorsally and branch extensively in the dorsal neuropil. In WT neurons the primary neurite bifurcates at the dorsal midline, while undead neurons are unable to bifurcate and turn to one side (orange arrowheads). In *H99/XR38* flies which contain both WT and undead neurons, the primary neurite to one side is thicker (orange arrowhead). Both WT and undead neurons join thoracic nerves (white arrows). Scale bars, 50 µm.

i, Reconstructed arborizations of undead neurons expressing CD8::GFP driven by *TDC2-GAL4* in flies bearing MARCM clones homozygous for the loss of function allele $dronc^{\Delta A8}$ (in which PCD is blocked). The 3D-rendered image is tilted at a 45° angle. Undead neurons have somata that are located at the ventral midline (orange arrowhead), branch extensively in the neuropil (green), have a turning primary neurite (orange), and project to the periphery through a thoracic nerve (arrow). Scale bar, 50 µm.

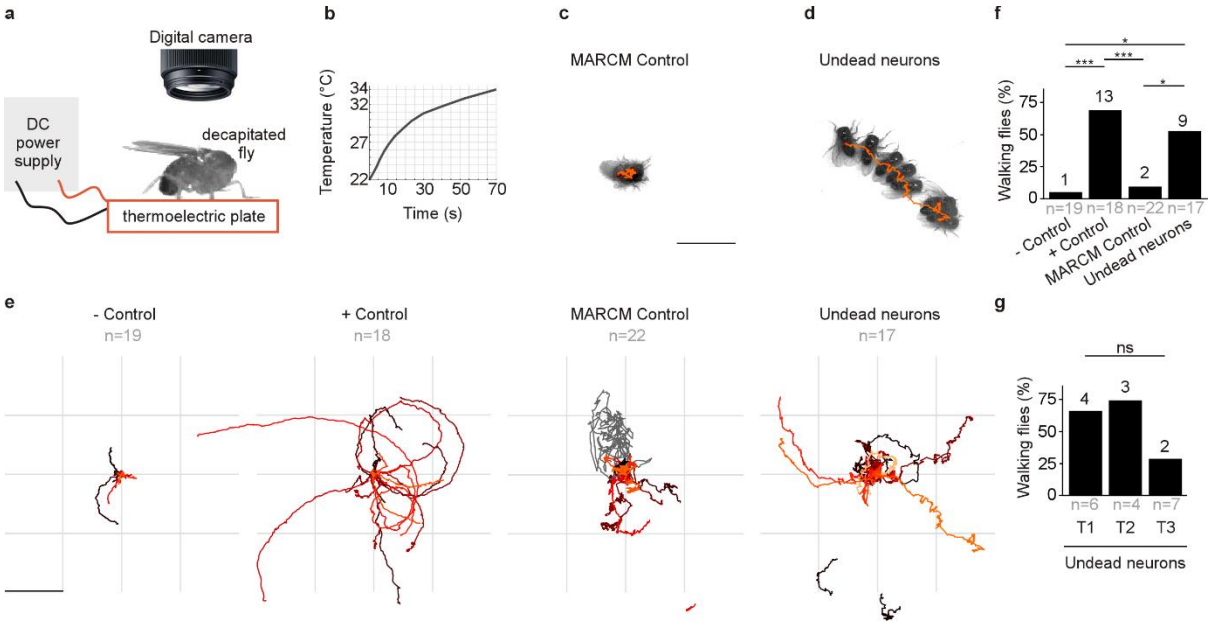

Figure 3 | Thermogenetic activation of undead neurons induces walking in decapitated *Drosophila*.

a, Schematic of behavioural assay with TrpA1 activation. Decapitated flies are placed on a thermoelectric plate connected to a DC power supply, exposed to a temperature ramp, and filmed from above using a digital camera.

b, Temperature ramp used for TrpA1 activation.

c, d, Example of a stationary MARCM Control fly (**c**). Example of a walking fly with undead neurons (**d**). Images represent maximum intensity projections of 13 frames at 0.3 fps tracing the centroid over time (orange line). Scale bar, 5 mm.

e, Fly body tracks generated by identifying the geometric centre of the fly body in each frame and storing the centre coordinates, plotted as a continuous line, one for each fly (walking or stationary) for negative controls (*UAS-TrpA1*), positive controls (*TDC2>TrpA1*), MARCM control flies and flies with MARCM clones of Undead neurons. Each trace represents one individual fly. Scale bar, 5 mm.

f, Quantification of the percentage of flies that walked per experimental group. *P**** = 0.0002 for negative versus positive control, *P**** = 0.0002 for positive controls versus MARCM Control, P* = 0.0242 for MARCM control versus undead neurons, *P** = 0.0135 for negative control versus undead neurons, Pearson's chi-squared corrected for multiple comparisons using a Bonferroni correction. *n* = 19 for negative controls, *n* = 18 for positive controls, *n* = 22 for MARCM control, *n* = 17 for undead neurons. *n* numbers for each group are given below and the number of flies which walked is shown above each bar.

606 **g**, Quantification of the number of walking undead neuron flies split into 3 anatomical
607 subgroups according to the location of MARCM clones in T1, T2, or T3. P^{ns} = 0.2628,
608 Pearson's chi-squared. n = 6 for T1, n = 4 for T2, n = 7 for T3. Numbers at the base are the
609 number of walking flies. The percentage is shown above each bar.

610

611

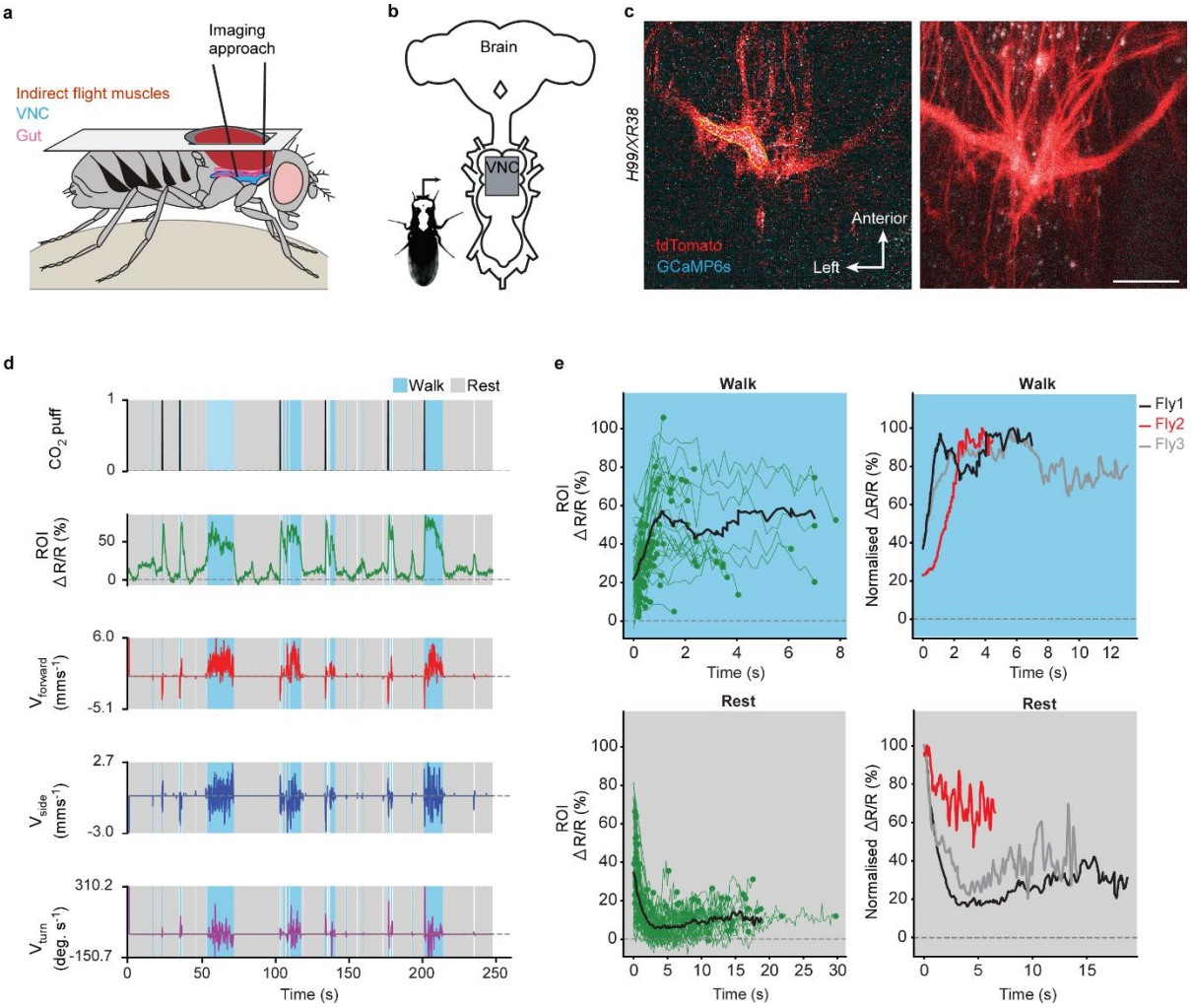

Figure 4 | Undead neurons are active during walking in intact adult *Drosophila*.

a, Schematic of the dorsal thoracic dissection and approach for ventral nerve cord functional imaging in tethered, adult flies.

b, The location of the imaging region of interest (grey box) with respect to a schematic of the adult CNS.

c, Raw 2-photon image of *TDC2-GAL4-positive* neurons co-expressing tdTomato (red) and GCaMP6s (cyan) in *H99/XR38* flies (**left**). Region-of-interest used to calculate %ΔR/R is outlined (yellow). Standard deviation z-projection of a dorsal-ventral image stack of the functional imaging region-of-interest in **b** (**right**). Scale bar, 50 µm.

d, Representative behavioural and functional imaging data in *H99/XR38* flies. Shown are: CO_2 stimulation (black), %ΔR/R (ratio of GCaMP6s / tdTomato) signal (green), and ball rotations indicating forward walking (red), sideways walking (blue), and turning (purple). The behaviour of the fly was classified as either walking (light blue), or resting (gray) by applying a threshold on ball rotation speed.

e, left Individual (green) and average (black) %ΔR/R traces within each behavioral epoch for walking (n = 82) and resting (n = 86) events processed from 750 s of imaging data . Solid green circles indicate the end of a behavioral epoch. The average trace (black line) was calculated for only periods with 4 or more traces. (**right**) Normalised average %ΔR/R traces for three different flies during walking and resting. The average (black) trace is the same as in the left panel.

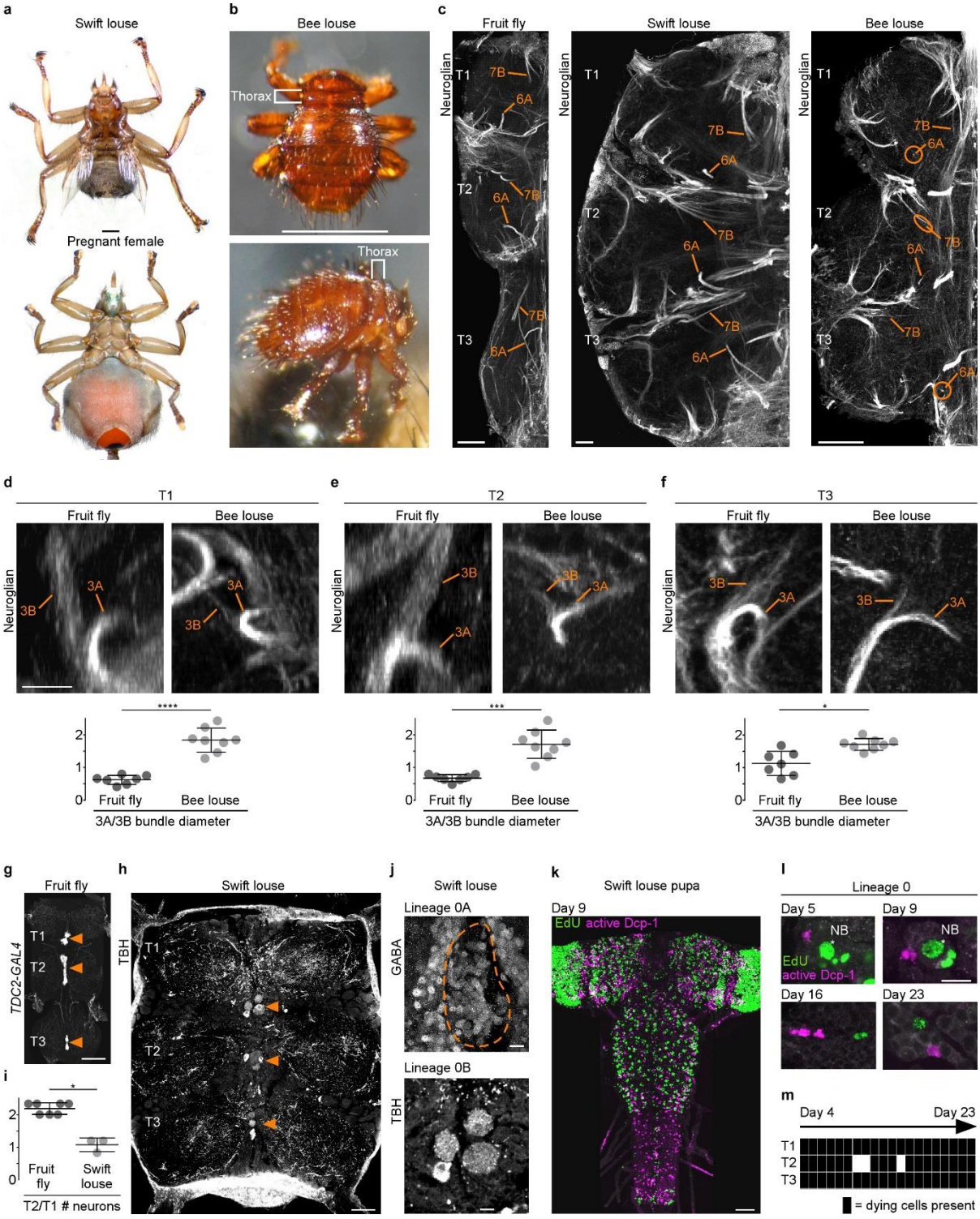

Figure 5 | Adaptive changes in the pattern of programmed cell death in flightless dipterans.

a, Dorsal view of an adult swift louse with vestigial wings (**top**). Ventral view of a female pregnant with a prepupa (**bottom**). Scale bar, 1 mm.

b, Dorsal (top) and side view (bottom) of an adult bee louse with a reduced thorax lacking wings and halteres. Scale bar, 1 mm.

c, Hemilineage VNC fiber tracts labelled with Neuroglian in a fruit fly (**left**), a swift louse (**middle**) and a bee louse (**right**). Shown are hemilineages 6A and 7B which are reduced in the bee louse in all three thoracic segments (T1, T2, T3). Scale bars, 50 µm.

d, **e**, **f**, 3A and 3B hemilineage fiber tracts labelled with Neuroglian in a fruit fly (**top left**) and a bee louse (**top right**). Shown are maximum intensity projections, chosen to best display hemilineages, from cross-section (T1 and T2) and frontal perspectives (T3). Quantifications of 3A/3B hemilineage bundle diameter ratios in fruit flies and bee lice are given below (P**** < 0.0001 in T1, independent samples t-test, P*** = 0.0001 for T2, Welch's t-test, P* = 0.0044, Welch's t-test. n = 7 fruit flies each, n = 8 bee lice each). Bars represent mean ± standard deviation.

g, Wild-type octopaminergic neurons in hemilineage 0B in a *Drosophila melanogaster* VNC labelled with CD8::GFP driven by *TDC2-GAL4* (orange arrowheads). Scale bar, 50 µm.

h, Octopaminergic neurons in hemilineage 0B in a swift louse VNC labelled with antibodies for tyramine β-hydroxylase (TBH, orange arrowheads). Fluorescence in the neuropil is derived from secondary antibodies trapped in the tracheal system and does not mark the true presence of TBH protein. Scale bar, 50 µm.

i, Quantification of T2/T1 number of octopaminergic neurons in fruit flies and swift lice shows that swift lice have lost the T2-specific higher numbers typical of flying dipterans (P* = 0.012, Mann-Whitney. n = 7 fruit flies, n = 3 swift lice). Bars represent mean ± standard deviation.

j, Cluster of cell bodies belonging to hemilineage 0A (dashed outline) labelled with antibodies for GABA (top) and cell bodies belonging to hemilineage 0B labelled with TBH antibodies (bottom) in the prothorax (T1) of a swift louse.

k, EdU labels proliferating cells and antibody-labelling for active Dcp-1 reveals dying cells in the CNS of a swift louse pupa 9 days after pupariation. Scale bar, 50 µm.

l, Dying cells in lineage 0 labelled with antibodies for active Dcp-1 located close to proliferating cells (e.g., NB*) throughout neurogenesis at Day 5 (**top left**), Day 9 (**top right**), Day 16 (**bottom left**) and Day 23 (**bottom right**) after pupariation. Scale bar, 10 µm. n = 1 each.

m, The occurrence of active Dcp-1-positive cells in lineage 0 in T1, T2 and T3 from Day 4 to Day 23 after pupariation in swift louse pupae (n = 1 each). Each black box indicates one occurrence.

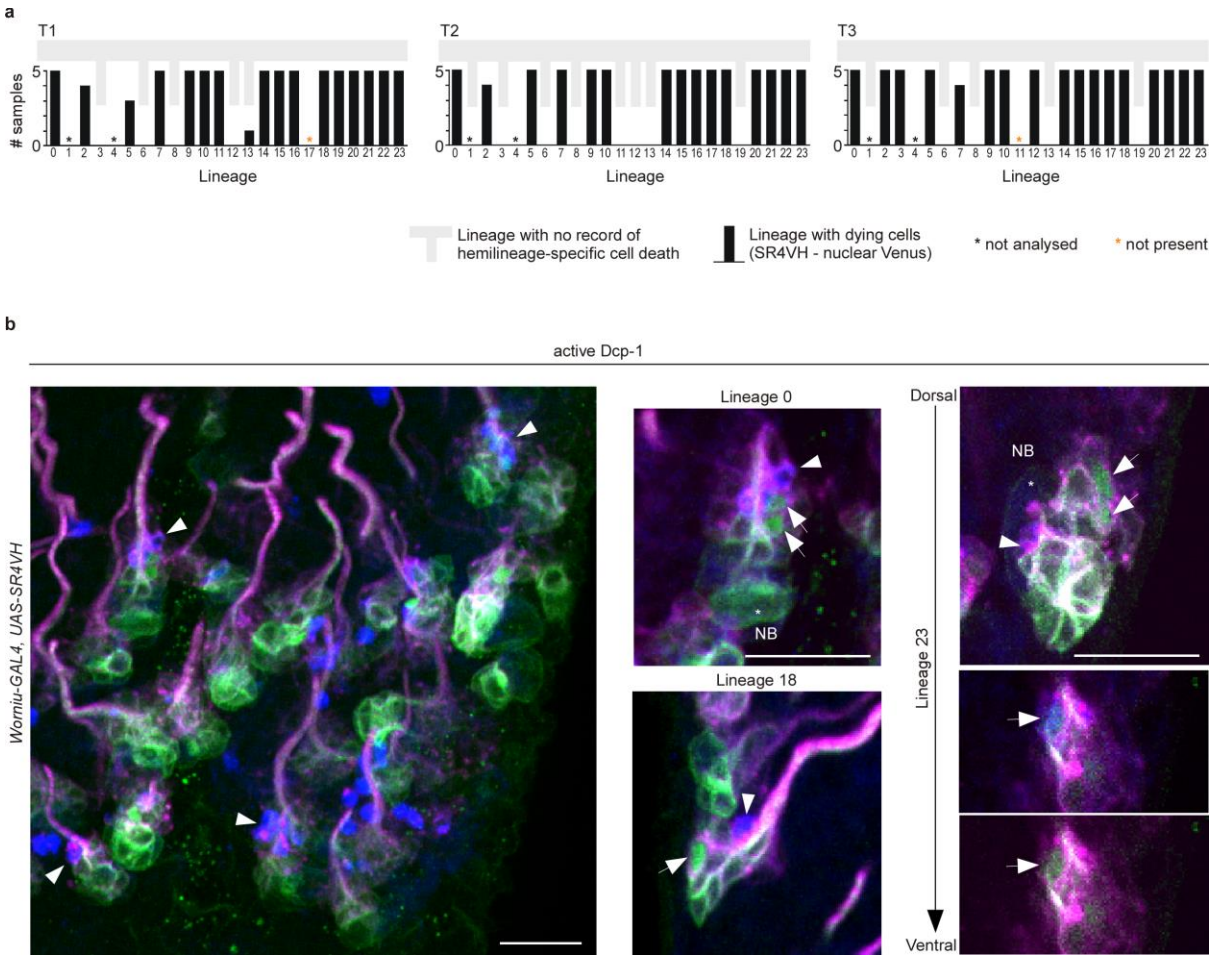

Extended data Figure 1 | SR4VH reveals successive stages of cell death in lineages with doomed hemilineages

a, Quantification of lineages with dying cells as reported with SR4VH in each thoracic segment from 5 wandering 3rd instar larvae. Back bars represent the number of samples in which dying cells were encountered in at least one hemisegment for that lineage. Grey bars represent lineages with no record of hemilineage-specific cell death as reported in Truman et al., 2010.

b, Antibodies for active Dcp-1 label cells located close to the lineage bundle in doomed lineages from larvae expressing SR4VH driven by *Worniu-GAL4*. Right panels show examples of doomed lineages 0, 18 and 23 containing cells at subsequent stages of cell death. White arrows indicate: nuclear Venus without cleaved Dcp-1 (early-stage), Venus and Dcp-1 colocalization (mid-stage), and pyknotic cells/dead cell membranes with RFP and cleaved Dcp-1 (late-stage). Scale bars, 10 µm. $n = 7$.

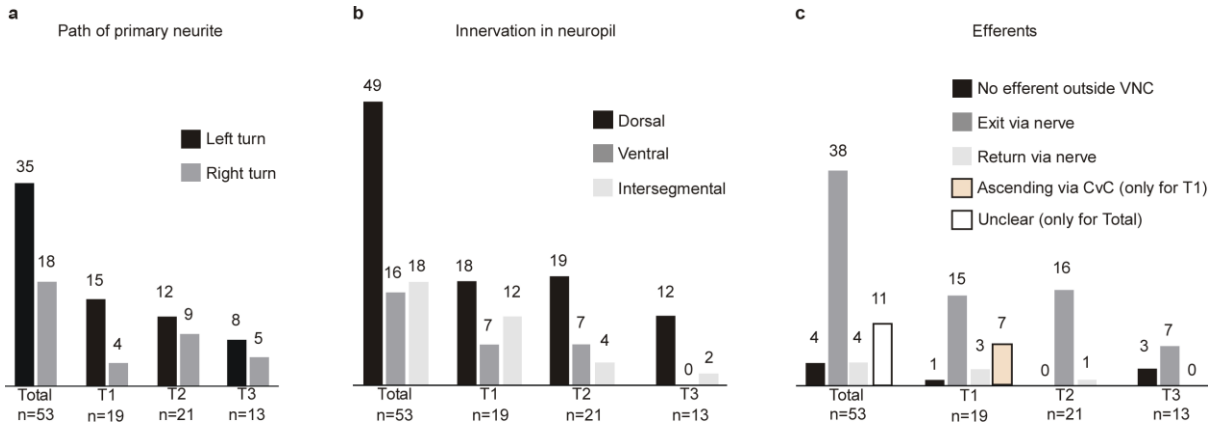

Extended data Figure 2 | Quantification of undead neuron morphology

a, Quantification of the primary neurite path. Most undead neurons arborize to the left.

b, Quantification of neuropil innervation. Most undead neurons branched extensively in the dorsal neuropil. Metathoracic (T3) undead neurons never innervated the ventral neuropil. Few undead neurons from each thoracic segment projected neurites into adjacent segments.

c, Quantification of efferent neurites. Most undead neurons joined a thoracic nerve heading towards the periphery. Some undead neurons in the prothoracic neuromere (T1) sent branches through the cervical connective (CvC).

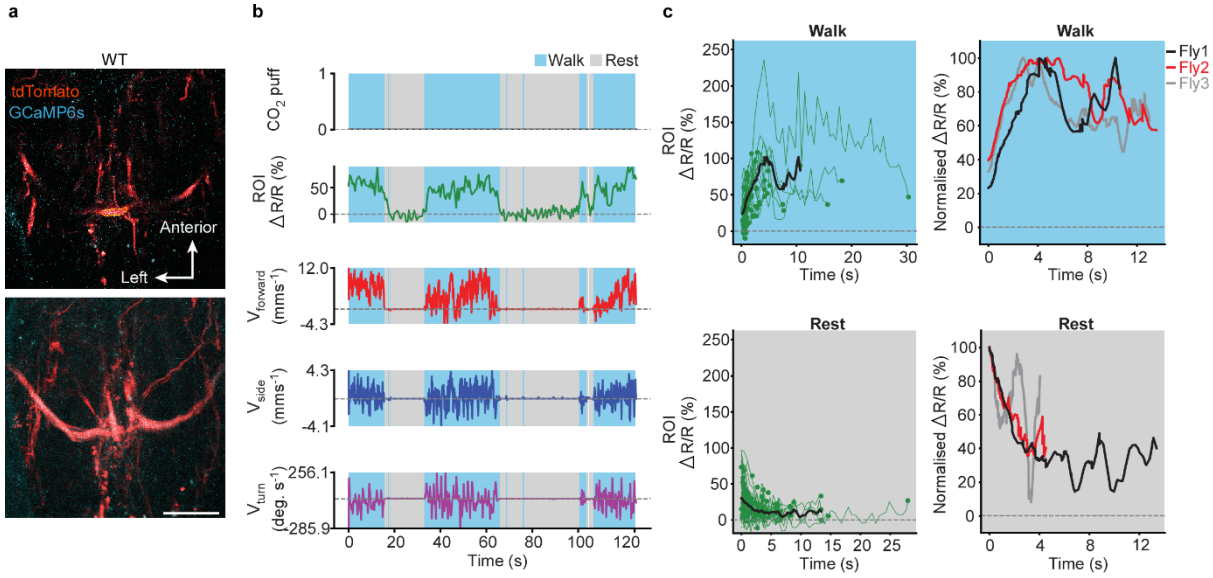

730

731 **Extended data Figure 3 | Wild-type octopaminergic neurons are active during walking in**
732 **intact adult *Drosophila*.**

733 **a,** Raw 2-photon image of *TDC2-GAL4-positive* neurons co-expressing tdTomato (red) and
734 GCaMP6s (cyan) in wild-type flies (**top**). Region-of-interest used to calculate %ΔR/R is
735 outlined (yellow). Standard deviation z-projection of a dorsal-ventral image stack of the
736 functional imaging region-of-interest in **b** (**bottom**). Scale bar, 50 µm.

737 **b,** Representative behavioural and functional imaging data in wild-type flies. Shown are: CO_2
738 stimulation (black, no stimulation), %ΔR/R (ratio of GCaMP6s / tdTomato) signal (green), and
739 ball rotations indicating forward walking (red), sideways walking (blue), and turning (purple).
740 The behaviour of the fly was classified as either walking (light blue), or resting (gray) by
741 applying a threshold on ball rotation speed.

742 **c, left** Individual (green) and average (black) %ΔR/R traces within each behavioral epoch for
743 walking (n = 77) and resting (n = 80) events processed from 720 s of imaging data . Solid green
744 circles indicate the end of a behavioral epoch. The average trace (black line) was calculated for
745 only periods with 4 or more traces. (**right**) Normalised average %ΔR/R traces for three
746 different flies during walking and resting. The average (black) trace is the same as in the left
747 panel.

748

749

750

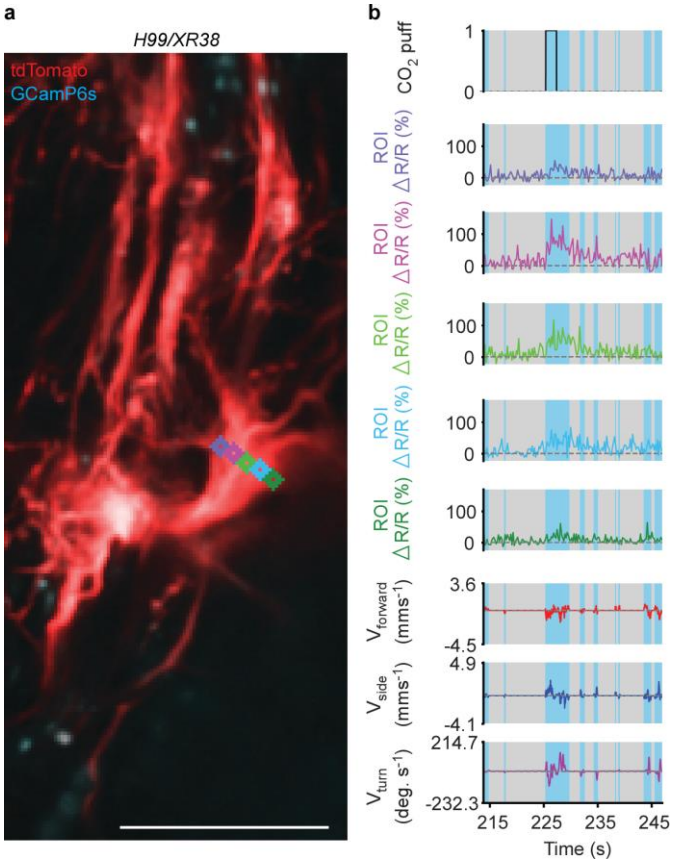

Extended data Figure 4 | Subregion analysis of calcium signals along the width of a primary neurite in a *H99/XR38* animal

a, Time-averaged projection of the imaging plane for *TDC2-GAL4*-positive neurons co-expressing tdTomato (red) and GCaMP6s (cyan) in a *H99/XR38* animal. Regions-of-interest used to calculate %ΔR/R (color-coded) are overlaid on top of time-projected and optic flow registered 2-photon images. Scale bar, 50 µm.

b, Representative behavioural and functional imaging data for this animal. Shown are: CO_2 stimulation (black), %ΔR/R (ratio of GCaMP6s / tdTomato) signal (color-coded for each ROI as in panel **a**), and ball rotations indicating forward walking (red), sideways walking (blue), and turning (purple). The behaviour of the fly was classified as either walking (light blue), or resting (gray) by applying a threshold on ball rotation speed.

Supplementary video 1 | Video recordings of control and 'undead' decapitated flies during thermogenetic activation

Examples from each behavioural category showing responses to heat-activation in negative control (top left), positive control (top right), MARCM control (bottom left) and undead neurons (bottom right). MARCM control and undead neuron animals were used for extracting the centroid trace provided in **Figure 3c**, **d**. The increase in temperature is displayed in the bottom right corner. Frames represent recordings from 30 to 70s.

Supplementary video 2 | Recording of 2-photon calcium imaging in undead neurons

Synchronized front and side camera behavior videography (**bottom-right**), and 2-photon imaging data (**top-right**) used for the data analysis provided in **Figure 4**.

Supplementary video 3 | Z-stack of the imaging area for GCaMP6s activity in undead neurons

A videography showing the imaging plane at different depths of the prothoracic segment corresponding to **Figure 1c.** The thicker left branch likely includes mostly undead neurons.

Supplementary Video 4 | Subregion neuronal activity patterns during walking

Imaging data used for analysis in **Extended data Figure 4**. Shown are %ΔR/R traces for ROIs marked in **Extended data Figure 4.**